Surfaces and Interfaces 73 (2025) 107514

Contents lists available at ScienceDirect

Surfaces and Interfaces

journal homepage: www.sciencedirect.com/journal/surfaces-and-interfaces

Functionalization of nanoporous poly (L-lactic acid) microspheres using light-activated chlorine dioxide radical gas

Hasinah Rafiq, Yu-I Hsu *, Hiroshi Uyama *

Department of Applied Chemistry, Graduate School of Engineering, Osaka University, Suita, Osaka 565-0871, Japan

ARTICLE INFO

Keywords:
Nanoporous PLLA microspheres
Surface oxidation
Chlorine dioxide radical gas
TBO dye adsorption
CO_2 adsorption
Hydroxyapatite deposition

ABSTRACT

Nanoporous polymer microspheres fabricated from biodegradable and biocompatible polymers such as poly (L-lactic acid) (PLLA) are excellent candidates for bone tissue engineering due to their high surface area and porosity. However, nanoporous surfaces often exhibit high hydrophobicity, and the lack of functional groups on PLLA limits their ability to support the efficient biomineralization process required for bone tissue engineering. In this study, we report a mild and non-destructive surface oxidation method to functionalize the surface of nanoporous PLLA microspheres using light-activated chlorine dioxide ($ClO_2^{\bullet}$) radical gas. This gas-phase surface oxidation approach introduces polar functional groups onto the microsphere surface while preserving its nanoporous morphology. The oxidation process was optimized *via* X-ray photoelectron spectroscopy (XPS) and toluidine blue (TBO) dye adsorption studies. Scanning electron microscopy (SEM) and nitrogen adsorption-desorption isotherm measurements confirmed that the nanoporous structure remained largely intact post-oxidation. Importantly, the oxidized microspheres were successfully functionalized with carboxyl and hydroxyl groups and exhibited improved hydroxyapatite deposition upon immersion in modified simulated body fluid (mSBF). This work demonstrates a facile, non-destructive strategy for surface functionalization of nanoporous PLLA microspheres without sacrificing their nanoporous architecture, representing a crucial step towards developing nanoporous biomineralizable scaffolds for future bone tissue engineering applications.

1. Introduction

Polymer nanostructures have raised great interest in various applications, including immobilization of biologically relevant molecules, functional adsorption and separation materials, and implantable bioactive scaffolds. Nanoscale structures offer a larger surface area to aid the adsorption and separation of molecules and closely mimic extracellular matrices for biological applications compared to their flat counterparts [1–3]. Numerous natural and synthetic polymers, including polyhydroxyalkanoates (PHAs) and poly (L-lactic acid) (PLLA), have been fashioned into three-dimensional nanoporous structures, such as microspheres and nanofibers [4,5]. Among them, PLLA is an attractive choice due to its FDA-approved biocompatibility, suitable for producing materials focused on biological applications [6].

Bone tissue engineering applications require polymers that are not only biocompatible but have high porosity and are capable of promoting hydroxyapatite (HA) nucleation on their surface, as HA is the primary inorganic phase of the bone structure [7]. Polymer nanostructure is an attractive choice for preparing bone regeneration scaffolds, as it provides a high surface area and interconnected porosity to better mimic the natural nanoporous organic bone structure. Additionally, since the native bone structure naturally contains hydroxyapatite to provide mechanical strength, the HA nucleation ability of a nanoporous polymer is essential in developing biomineralizable polymer scaffolds that can potentially integrate with native bone tissues for bone tissue regeneration applications [8–12]. However, nanoporous PLLA materials are inherently hydrophobic and have low surface energy due to their rough surface and the bulky methyl groups on their polymer chains [13,14]. These properties impede efficient HA nucleation and biomineralization on the surface of the polymer nanostructures, as it results in poor hydrophilicity of the materials. Additionally, pristine PLLA lacks the polar functional groups, such as carboxyl and hydroxyl groups, that act as nucleating sites to attract Ca^{2+} for efficient hydroxyapatite deposition [10]. Hence, it is necessary to modify the surface of nanoporous PLLA materials as an important first step towards expanding their potential as nanoporous bone regeneration scaffolds.

Various strategies have been explored to modify the surfaces of polymer structures to enhance their hydrophilicity and to introduce

* Corresponding authors.
E-mail addresses: yuihsu@chem.eng.osaka-u.ac.jp (Y.-I. Hsu), uyama@chem.osaka-u.ac.jp (H. Uyama).

https://doi.org/10.1016/j.surfin.2025.107514
Received 23 April 2025; Received in revised form 19 July 2025; Accepted 24 August 2025
Available online 30 August 2025

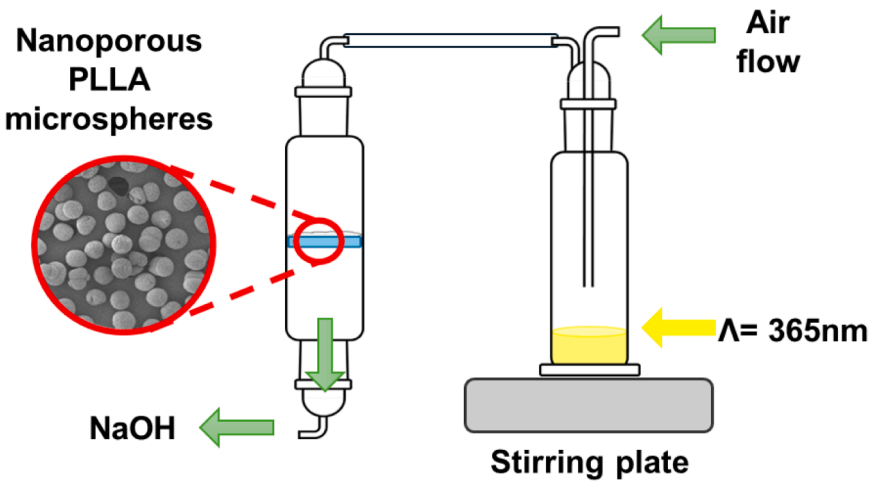

Fig. 1. Oxidation set-up for surface oxidation of PLLA microspheres using light-activated chlorine radical gas.

polymers with suitable reaction sites for functionalization. Techniques such as plasma treatment, laser ablation, and ion-beam illumination are commonly used to impart surface functionalities onto polymer surfaces without the need for solvents [15–17]. However, modification of polymer substrates *via* these approaches is usually accompanied by changes in the morphology of the polymers, such as corrugation, engravement, and surface roughening [18]. Moreover, the short interaction time between the modifying agent and the outermost surface of the polymer restricts the surface functionalization to flat or two-dimensional surfaces such as thin films, nanofibers, and membranes [19]. Additionally, these methods are used to introduce surface roughness on smooth polymer microparticles or microspheres alongside surface functionalization. As a result, the original morphology of these materials is often lost during the process [20].

On the other hand, wet-chemistry methods ensure homogeneous surface functionalization of three-dimensional polymer structures. Polymer materials are immersed in acidic or alkaline solutions to hydrolyze their surface to generate carboxyl and hydroxyl groups. The drawbacks of these methods are evident from the degradation of the surface of the porous polymer after modification [12]. Techniques such as diazonium chemistry and polydopamine coating favor surface modification of polymer materials without significant degradation [19,21]. Nevertheless, the exploration of these techniques for modifying the surface of nanoporous PLLA material is relatively rare, with limited studies addressing their effectiveness in modifying delicate nano-architectures without significant morphological change for further applications, especially in bone tissue engineering applications.

To address these limitations, we first prepared nanoporous PLLA microspheres and utilized light-activated chlorine dioxide radical ($ClO_2^{\bullet}$) gas to functionalize the surface of nanoporous PLLA microspheres without compromising their nanoporous architecture. Chlorine dioxide radical ($ClO_2^{\bullet}$) gas acts as an effective C—H bond oxygenation agent to effectively introduce polar functional groups on the surface of many polymers, including PLLA [22–24]. The ($ClO2^{\bullet}$) gas is generated by irradiating an acidified solution of sodium chlorite ($NaClO_2$) to generate chlorine ($Cl^{\bullet}$) radical gas. The $Cl^{\bullet}$ radicals in gaseous form can easily pass through the PLLA microspheres, and upon contact with its surface polymer chains, the radicals cleave the C—H bonds on the surface to form methyl radicals. The methyl radicals form oxygenated products with the subsequent addition of singlet oxygen to form PLLA materials functionalized with carboxyl and hydroxyl groups [24,25].

In this study, we first optimized the surface functionalization process by evaluating the effect of oxidation time and illumination intensity of the UV light on the elemental ratios, concentration of surface functional groups, and concentration of carboxyl groups on the surface of PLLA microspheres *via* XPS and toluidine blue O (TBO) dye adsorption measurements. The preservation of surface nanoporosity after surface oxidation was evaluated using SEM imaging and BET adsorption measurements. Additionally, the surface reactivity of the newly introduced polar functional groups was further assessed through CO_2 adsorption measurements. The CO_2 adsorption was used as an indirect probe of surface polarity after oxidation, as previous work had outlined the enhancement of CO_2 adsorption of porous materials due to the presence of carboxyl groups. As a result, the presence of polar functional groups on the surface of nanoporous PLLA microspheres increases the HA nucleation ability upon immersion in modified simulated body fluid.

Overall, this study outlined a facile surface modification method using light-activated chlorine dioxide radical to effectively oxidize and introduce polar functional groups onto nanoporous PLLA microspheres. The gas-phase oxidation process preserves the delicate nanoporous architecture of the PLLA microspheres. Most importantly, our results demonstrate the ability of this non-destructive surface modification method to prepare functionalized nanoporous microspheres with enhanced biomineralization ability. All in all, this approach represents a key first step towards developing nanoporous bioactive scaffolds for potential bone tissue engineering applications.

2. Experimental section

2.1. Materials

Poly (l-lactic acid) (PLLA, Ingeo™ Biopolymer 4032D) was purchased from Nature Works (Minnesota, USA). 1,3-dioxolane, 2-butanone, ethanol, and isopropyl alcohol (IPA) were purchased from Nacalai Tesque Inc. (Kyoto, Japan) and were used as received. Sodium chlorite ($NaClO_2$) and toluidine blue O (TBO) dye were obtained from Sigma-Aldrich. Concentrated hydrochloric acid was purchased from FUJIFILM Wako Pure Chemical Corporation. The salts used for the preparation of the modified SBF solution, NaCl, KCl, $MgSO_4$, $MgCl_2$, $NaHCO_3$, $CaCl_2$, and KH_2PO_4, were purchased from Wako Chemicals.

2.2. Preparation of nanoporous PLLA microspheres

Nanoporous PLLA microspheres with diameters around 49.4 ± 2.8 μm were prepared as outlined in previous research [14]. In brief, 10 g of PLLA was dissolved at a fixed concentration of 10 % w/v in a 100 mL ternary solvent system of 1,3-dioxolane/2-butanone/water. The ratio of the ternary solvent system was kept at 10/85/5. A homogenous polymer solution was obtained after stirring for 2 h. The PLLA solution was then poured into a glass container placed in an ice bath and quenched for another 2 h to form a gel-like solution. The gel-like solution was then sonicated and added to excess isopropyl alcohol for solvent exchange for

Table 1
Composition of modified SBF (mSBF) solution.

Reagent	Concentration (mM)
NaCl	141
KCL	4.0
$MgSO_4$	0.5
$MgCl_2$	1.0
$NaHCO_3$	4.2
$CaCl_2$	2.5
KH_2PO_4	1.0

2 days, followed by vacuum filtration. The collected microspheres were then dried under vacuum for 8 h until a constant weight was obtained. The nanoporous PLLA microspheres in powder form were stored in a desiccator until further use.

2.3. Surface oxidation of nanoporous PLLA microspheres

250 mg of dry PLLA nanoporous PLLA microspheres were placed into a glass filter tube, and the oxidation set-up was assembled as shown in Fig. 1. An aqueous solution of 200 mg of $NaClO_2$ in 14 mL deionized water and 0.2 mL HCL was prepared beforehand and placed into a gas wash. The gaseous oxidizing agent consisting of ($ClO2^{\bullet}$) gas was then generated by irradiating the solution in the gas wash with UV light from PiPhotonics (Shizuoka, Japan, HOLOLIGHT KAKU Lamp, λ=365 nm). The gas flowed through the PLLA microspheres using a CHIKARA α1500 pump from NISSO (Osaka, Japan) at 1.0 L/min. The aqueous oxidizing solution was replaced every 20 min to ensure a continuous supply of oxidizing gas. The PLLA nanoporous microspheres were redispersed using a vortex every 10 min to ensure homogeneous oxidation. After oxidation was completed, the PLLA microspheres were collected and washed with 5 % ethanol solution and water, respectively, and freeze-dried for 3 days.

2.4. TBO dye adsorption capacity for quantification of carboxyl groups

The cationic TBO dye adsorption test is a widely used method for the quantification of carboxyl groups on the surface of polymer, as it interacts electrostatically with negatively charged carboxylic groups at a basic pH at 1:1 molar ratio [26]. 20 mg of PLLA microspheres were dispersed in 1 mL of toluidine blue O (TBO) dye solution (15 mg/L) at pH 10. The solution was then sonicated for 10 min and placed in a Bioshaker for 1 h to ensure complete dye adsorption. The PLLA microspheres were removed, and the supernatant was analyzed at 630 nm using a microplate reader (SH9000LAB; Corona Electric Co., Ltd., Ibaraki, Japan). A standard solution of TBO at different concentrations was prepared to build a calibration curve (Fig. S1). Using this calibration curve, the concentrations of the TBO solutions before and after dye adsorption were determined. The adsorption capability was assessed based on the concentration difference before and after the adsorption process. Subsequently, the dye adsorption capacity was calculated based on the equation below.

$$q_e = (C_o\text{-}C_t)V/m \quad (1)$$

where q_e is the equilibrium adsorption capacity (mg/g), V is the volume of solution (mL), m is the mass of microspheres used (mg) and C_0 and C_t are the initial and final (equilibrium) concentrations.

2.5. Biomineralization of nanoporous PLLA microspheres

50 mg of PLLA microspheres were dispersed in 10 mL of simulated body fluid (mSBF) and incubated for 7 days at 37 °C to induce hydroxyapatite growth. The mSBF solution was replaced with a freshly prepared solution daily to ensure appropriate ionic concentrations for hydroxyapatite growth. After 7 days, the microspheres were collected and washed repeatedly with distilled water and finally freeze-dried for 3 days. The mSBF was prepared by dissolving the following reagents in 1L of deionized water, as outlined in Table 1. The pH of the solution is held at pH = 6.8 to avoid precipitation of CaP phases. Compared to a typical SBF solution, the concentration of $CaCl_2$ and KH_2PO_4 is doubled in amount.

2.6. Characterization

The surface elemental composition of unoxidized and oxidized PLLA microspheres was analyzed using XPS (XPS, JPS-9010MC, JEOL, Tokyo, Japan). The X-ray source under standard conditions was operated at 12 kV and 15 mA. The atomic ratio concentration and the peak fitting of the high-resolution XPS spectra of C1s were performed using the CasaXPS Version 2.3.25 software. The chemical compositions and functional groups were determined by an ATR-FTIR (FT/IR4700, JASCO) at room temperature with a diamond window. All spectra were acquired at 4 cm^{-1} resolution over 100 scans in the scan range of 500–4000 cm^{-1}. The elemental composition of mineralized PLLA microspheres was captured by Energy Dispersive X-ray spectroscopy (EDX) (HITACHI, Miniscope TM 3000 equipped with Swift ED 3000). Powder XRD patterns of the microspheres before and after mineralization were obtained using SmartLab (Rigaku Corporation, Tokyo, Japan) with a Cu K-beta X-ray source and a scanning speed of 2° min −1 over a 2θ range of 5–50° The wettability of the microspheres was studied with a WCA test using a Drop Master DM300, Kyowa Interface Science, Tokyo, Japan, with the FAMAS basic software.

The morphologies of the microspheres were characterized by SEM using the SU3500 device (Hitachi). The sample was coated with Au–Pd by placing it in a vacuum chamber for 3 min and sputtering the surface using an ion sputter apparatus (E-1010, Hitachi, Tokyo, Japan) at 1.0 Torr and 15 mA of electric current. The average diameter of microspheres was calculated using ImageJ software by measuring the width of 30 individual microspheres at various locations of the sample. Before analysis, the pixel-distance ratio was set based on the known scale bar on the SEM image. Nitrogen adsorption/desorption isotherms were recorded using a NOVA 4200e surface area and pore size analyzer (Quantachrome Instruments) at 77 K. Before the measurements, the sample was freeze-dried for 3 days and then degassed at 40 °C under vacuum for 12 h. The specific surface area and pore size distribution were calculated using the Brunauer–Emmett–Teller (BET) equation and the DFT method.

Thermal characteristics of PLLA microspheres were analyzed using a differential scanning calorimeter (EXSTAR 6000 DSC6220, SEIKO, Tokyo, Japan) at a temperature range of 30–200 °C at a heating rate of 10 °C/min under an N_2 atmosphere. The amount of heat required to melt PLLA (ΔH_m) was quantified from the area under the curve of melting temperature (T_m). The estimation of the crystallinity of PLLA microspheres was calculated using the theoretical heat of fusion of 100 % crystallized PLA (93.1 J/g) by using the following equation:

$$Xc = (\Delta H_m/(\Delta H_m^0) \text{ x } 100\ \% \quad (2)$$

where ΔH_m and ΔH_m^0 are the heat of the fusion of PLLA microspheres and the 100 % crystalized PLLA, respectively. Thermal stability analysis was done with STA7000 Thermogravimetric Analyzer (Hitachi, Japan) by applying the heating rate of 10 °C in an inert nitrogen atmosphere (from 30 to 600 °C).

The number average molecular weight (Mn) and the weight average molecular weight (Mw) of the PLLA microspheres were determined The molecular weight of the PLLA microspheres' surface was measured by Gel Permeation Chromatography (GPC) using HLC-8420 GPC (Tosoh, Tokyo, Japan) with chloroform as the solvent. Molecular weight was calculated with a calibration curve derived from polystyrene standards with chloroform as the eluent flowing ratio at 0.5 mL min^{-1} and a sample concentration of 10.0 mg mL^{-1}.

Table 2
Oxidation conditions of PLLA microspheres.

PLA samples	Oxidation time (min)	Illumination intensity (mW)
20 min 20 mW	20	20
40 min 20 mW	40	20
60 min 20 mW	60	20
60 min 30 mW	60	30
60 min 40 mW	60	40

3. RESULTS AND discussion

3.1. Surface oxidation of nanoporous PLLA microspheres

The effect of surface oxidation conditions on PLLA nanoporous microspheres was evaluated by preparing samples with different oxidation conditions, as summarized in Table 2. The surface oxidation of nanoporous PLLA microspheres was first optimized to obtain oxidized PLLA microspheres with sufficient polar functional groups and minimal surface degradation. Based on the previous research conducted by our research group on the functionalization of various polymers *via* $ClO_2^{\bullet}$ radical gas, the oxidation strength of the radical gas can be controlled by varying oxidation time and the illumination intensity of the UV light used to activate the acidified $NaClO_2$ aqueous solution. UV irradiation generates $ClO_2^{\bullet}$ radicals, and the oxidation strength is determined by the quantity of radicals contacting the polymer surface. Longer oxidation times allow greater radical–surface interaction, thereby increasing the degree of surface oxidation. On the same note, higher UV illumination intensity generates more $ClO_2^{\bullet}$ radicals per unit time, enhancing oxidation efficiency. However, prolonged exposure or excessively high

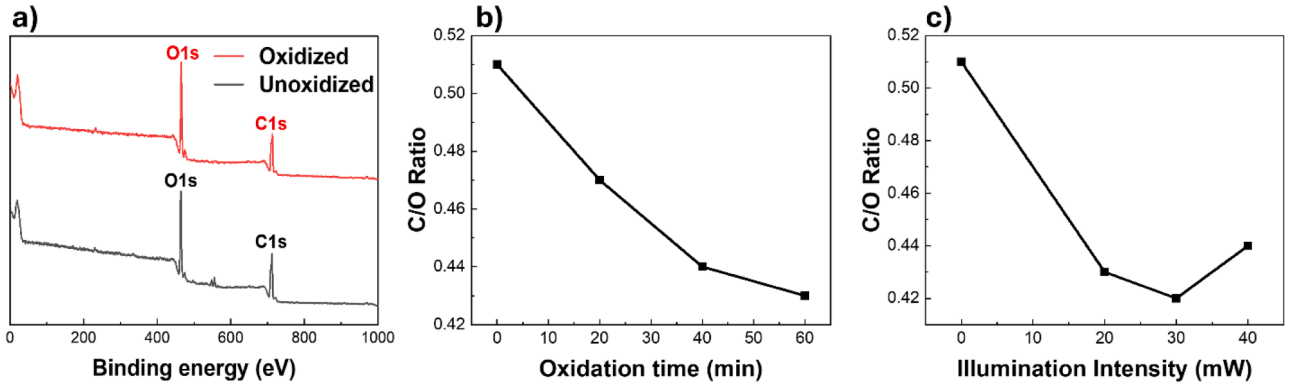

Fig. 2. XPS analysis: (a) Wide scans of unoxidized and oxidized PLLA microspheres (at 20 mW, 60 min). Elemental ratio, C/O of PLLA microspheres under (b) different oxidation times at 20 mW illumination intensity and (c) different illumination intensities at 20 min oxidation time.

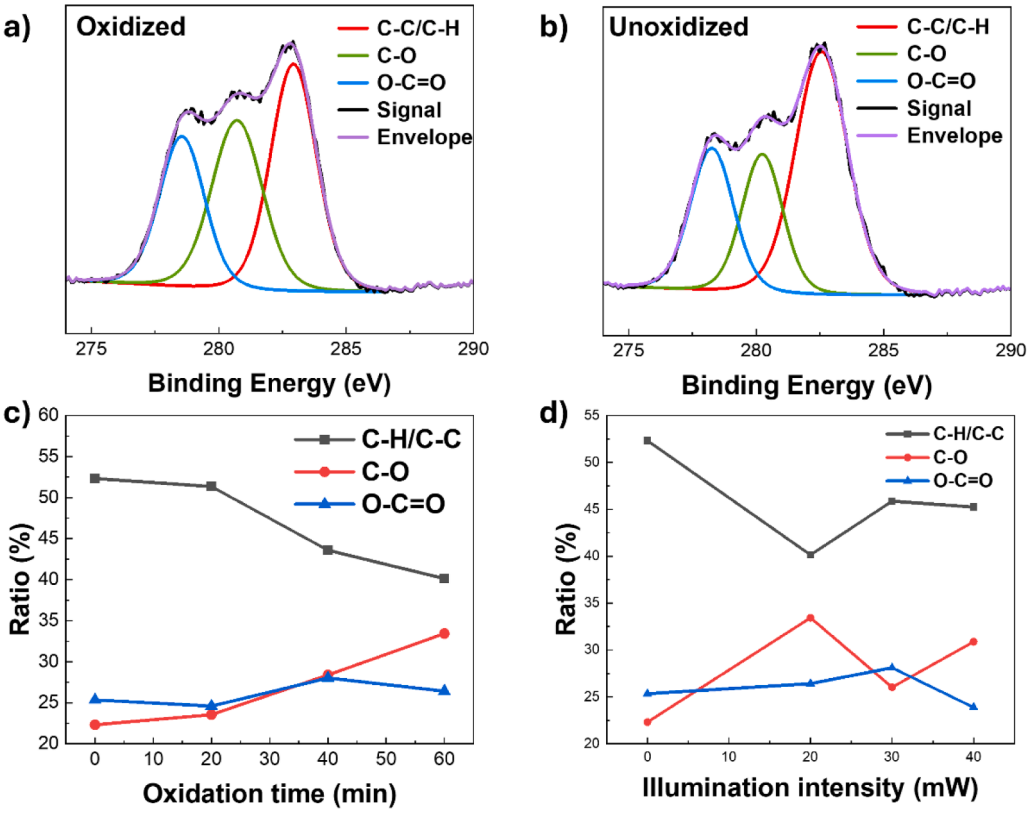

Fig. 3. C1s spectra of (a) unoxidized and (b) oxidized PLLA microspheres (20 mW 60 min). The ratio of functional group concentration of C—C/C—H, C—O, and *O* = *C*—O on the surface of PLLA microspheres under different (c) oxidation times and (d) illumination intensity.

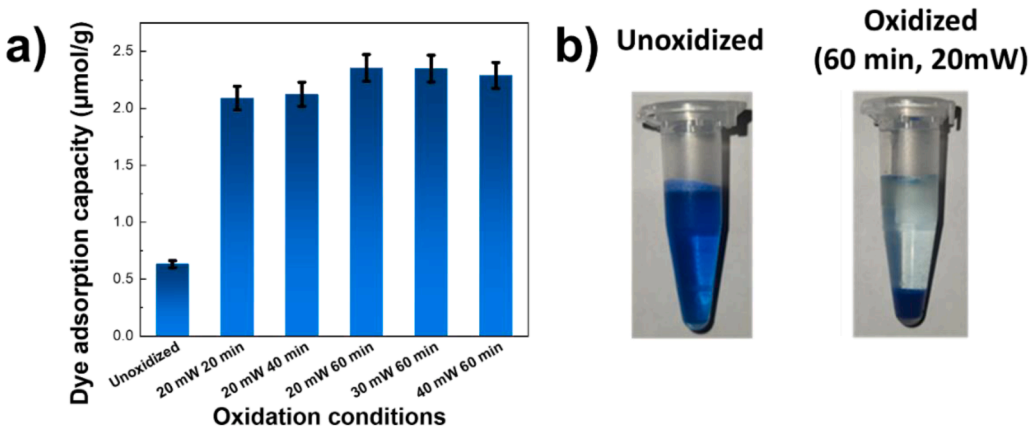

Fig. 4. a) Dye adsorption capacity of PLLA microspheres under different oxidation conditions and b) images of PLLA microspheres before and after dye adsorption tests.

illumination intensity is known to cause polymer surface degradation, such as surface erosion and even increased hydrophobicity due to over-oxidation and chain scission, which exposes more hydrophobic inner polymer chains after oxidation. Therefore, optimization is necessary to balance effective surface functionalization without excessive surface degradation.

To assess the effect of surface oxidation on PLLA microspheres, XPS was first employed in oxidized and unoxidized samples. The atomic ratio was analyzed using CasaXPS software to evaluate the effect of oxidation time and illumination intensity on the elemental composition of PLLA microspheres, and the results are summarized in Fig. 2 (a-c). The elemental ratio of C/O on the surface of neat PLLA microspheres was 0.51. After oxidation at 20, 40, and 60 min, the elemental ratio of C/O decreased to 0.47,0.44, and 0.43, respectively. However, when the illumination intensity increased from 20 mW to 30 and 40 mW for samples oxidized at 60 min, the C/O ratio showed an increase from 0.43 to 0.45 when the oxidation intensity was increased up to 40 mW.

The ratios of functional group concentrations were analyzed by performing curve fitting of the high-resolution C1s spectra from XPS measurements, as shown in Fig. 3 (a-b). The C1s spectra were fitted with three peaks assigned to binding energies of C—C (284.8 eV), C—O (286 eV), and O—*C* = *O* (289 eV), respectively. As summarized in Fig. 3(c), at a fixed illumination intensity of 20 mW, the ratio of C—H/C—C bonds on the surface of PLLA microspheres progressively decreased from 53.3 % to 40.1 % as the oxidation time increased from 0 min (unoxidized sample) to 60 min. Furthermore, the ratio of C—O and O—C = *O* increased from 22.3 % to 33.4 %, and from 25.4 % to 26.4 %, respectively.

On the other hand, the increase of illumination intensity from 20 mW to 30 and 40 mW at a fixed oxidation time of 60 min showed the opposite trend Fig. 3(d). As the illumination intensity increased, the ratio of C—H/C—C bonds on the surface of PLLA microspheres progressively decreased from 53.3 % to 40.1 % while the ratio of C—O and O—*C* = *O* increased from 22.3 % and 25.4 % to 33.4 % and 26.4 %, respectively. Additionally, there is an obvious decrease in the peak at 285 eV corresponding to C—C/C—H, accompanied by the increase in both C—O and O—*C* = *O* in the oxidized sample (20 mW, 60 min).

The increase in oxygen content on the surface of the PLLA microspheres after oxidation is due to the introduction of oxygen-containing functional groups such as hydroxyl and carboxyl groups, as explained by previous research [19]. When the oxidation time was increased from 20 min to 60 min, the contact time between the chlorine radical gas and the PLLA surface increased. As a result, more methyl groups were cleaved and subsequently replaced with oxygenated functional groups. However, as the illumination intensity increased from 20 mW to 30 and 40 mW, the amount of oxygenated functional groups decreased. As the acidified $NaCl_2O_4$ was illuminated with stronger UV light intensity, a higher amount of chlorine radical gas was generated during oxidation, which led to excessive oxidation of the polymer chain. The excessive cleaving of the polymer chain formed smaller polymer fragments that were easily removed during the washing process. As a result, it revealed the unoxidized, hydrophobic inner portion of the PLLA microspheres. Additionally, we attempted to characterize the change in functional groups of PLLA microspheres using ATR-FTIR after oxidation (Fig. S2), however, no significant differences were observed due to the overlapping of carbonyl groups with the robust ester peaks on the PLLA surface [24,25].

TBO dye adsorption tests were carried out to evaluate the correlation between oxidation conditions and the concentration of carboxyl groups introduced on the surface of PLLA microspheres, as TBO dye electrostatically adsorbs onto carboxyl groups at a 1:1 molar ratio [23]. As shown in Fig. 4(a), the number of carboxyl groups on the surface of oxidized PLLA microspheres showed around a 3.5-fold increase from 0.66 μmol/g to 2.35 μmol/g for the sample oxidized at 20 mW for 60 min. The TBO dye adsorption capacity increased as the oxidation time increased. However, no significant change was observed between 20 mW and 40 mW illumination intensities, suggesting that higher UV intensity does not markedly enhance functional group density under the tested conditions. The oxidized PLLA microspheres showed a significantly deeper color after the adsorption process compared to the unoxidized sample (Fig. 4(b)). Additionally, the oxidized PLLA microspheres sank to the bottom of the test tube after the adsorption test for 1 hour compared to the unoxidized sample (Fig. 4(b)), indicating enhanced hydrophilicity after being in contact with water for a prolonged period of time. Interestingly, in the dry state, the oxidized microspheres did not exhibit any significant improvement in water affinity compared to the unoxidized sample (Fig. S4). The powdery nanoporous PLLA microspheres repelled water droplets, preventing their stable formation on the surface. This behavior can be explained by the Cassie–Baxter wetting state, where air becomes trapped within the surface nanopores, creating a solid–air interface that minimizes the actual solid–liquid contact area [14]. Even though the oxidized microspheres possessed polar functional groups, the presence of entrapped air pockets and the rough surface dominated the wetting behavior, maintaining a highly hydrophobic state. However, after prolonged immersion during the adsorption test, water gradually penetrated the nanopores, which explained the sinking behavior of the oxidized microspheres in aqueous solution after 1 hour.

In short, the results of XPS measurements and TBO dye adsorption tests revealed the optimum parameters for the surface oxidation of PLLA microspheres to be at 20 mW illumination intensity and 60 min oxidation time. The dye adsorption test also revealed the enhanced hydrophilicity of nanoporous PLLA microspheres after oxidation, after prolonged immersion in aqueous solution.

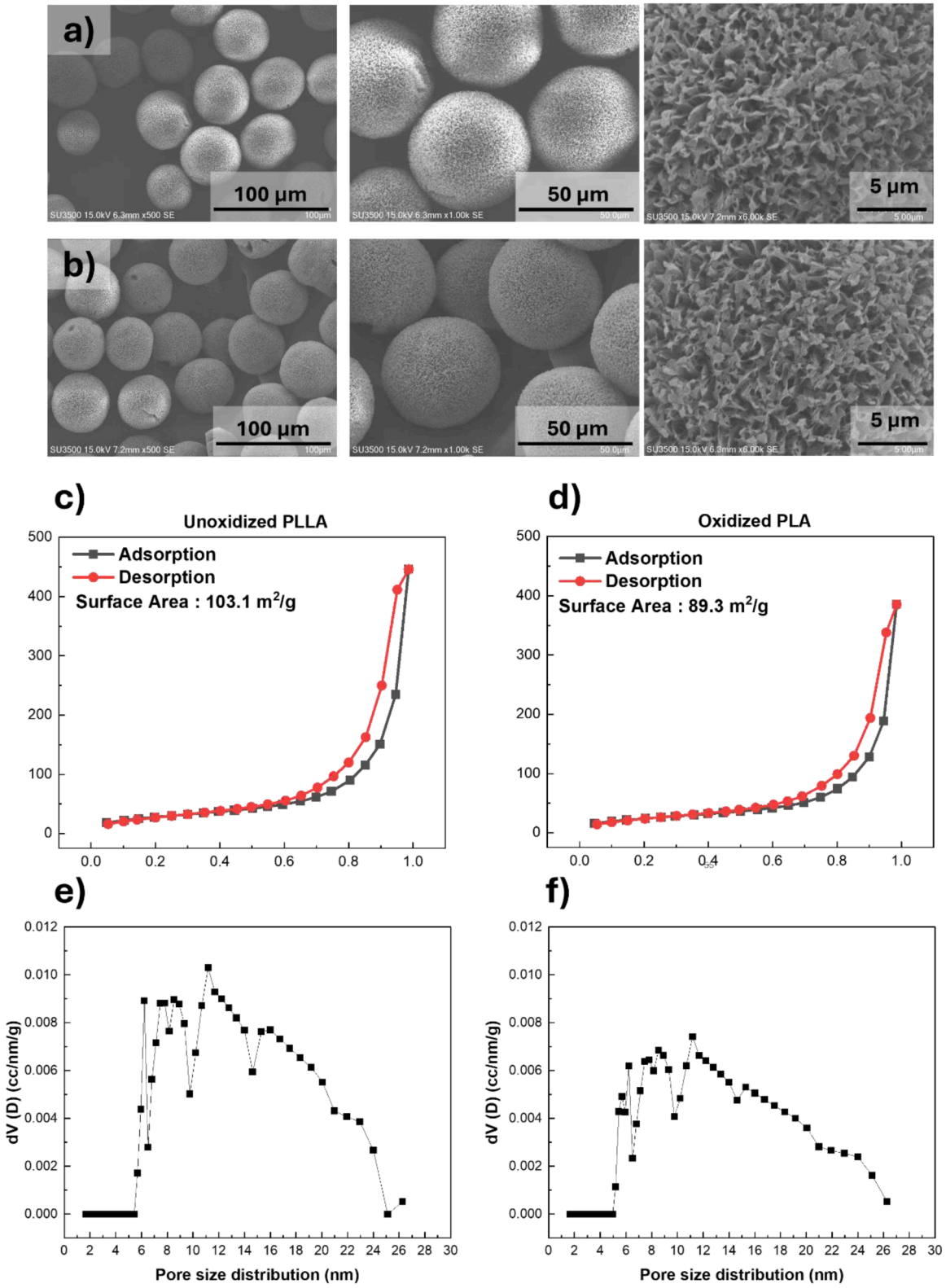

Fig. 5. (a-b) SEM images of PLLA microspheres before and after oxidation, (c-d) nitrogen adsorption-desorption isotherms, and (e-f) pore size distribution of PLLA microspheres before and after oxidation.

3.2. Surface characterization of nanoporous PLLA microspheres

The effect of surface oxidation on the nanoporous structure of PLLA microspheres was evaluated using scanning electron microscopy (SEM) and BET adsorption measurements. As shown in Fig. 5 (a-b), the PLLA nanoporous microspheres fabricated in this work exhibit a spherical shape with a nanoporous surface. The nanopores on its surface arise from the crystallization of polymer lamellae into spherulites due to the polymer crystallization process during the thermally induced phase separation process [14]. Based on these images, it is clear that the

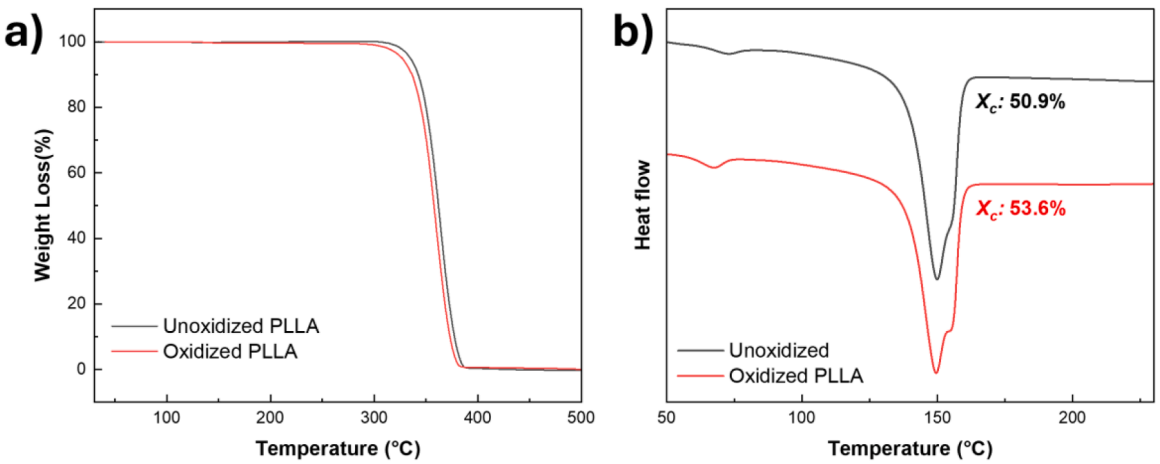

Fig. 6. a) TGA and b) DSC thermograms of oxidized and unoxidized microspheres.

surface oxidation process did not significantly alter the nanoporous morphology of the PLLA microspheres. As shown in Fig. 5 (c-d), the isotherm for both oxidized and unoxidized samples showed a Type IV hysteresis loop according to IUPAC classification, which confirms the presence of slit-like pores on the surface of PLLA microspheres [27]. The surface area decreased from 103.1 to 89.3 m^2/g, accompanied by a decrease in pore volume (0.53 to 0.49 mL/g) after oxidation. Both the oxidized and unoxidized PLLA microspheres have nanopores ranging from 5 to 26 nanometers, with average pore sizes of 11.1 and 11.2 nm, respectively (Fig. 5 (e-f)). Although the surface area and the pore volume of the PLLA microspheres showed a decrease, the presence of intact nanopores observed in SEM and the similar pattern of adsorption isotherms and pore size distribution confirms the mild and non-destructive nature of the surface oxidation process.

3.3. *Physical properties*

The surface modification of polymers *via* light-activated chlorine dioxide radicals induces the degradation of polymers alongside the introduction of polar functional groups. The oxidation process led to the degradation of PLLA microspheres as evidenced by a decrease in molecular weight after oxidation, particularly for samples with longer

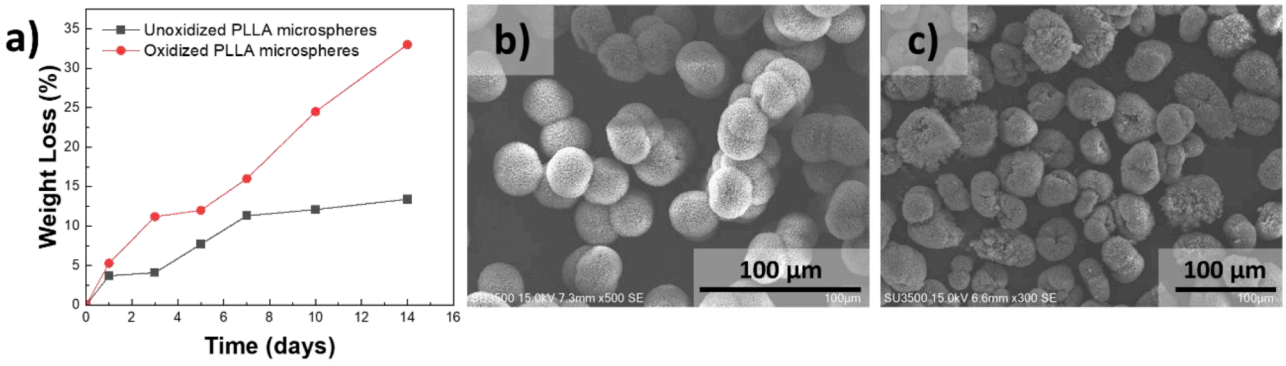

Fig. 7. a) Weight loss of unoxidized and oxidized PLLA microspheres after degradation in PBS buffer for 14 days. b) Morphology of PLLA microspheres after 14 days immersion in PBS buffer.

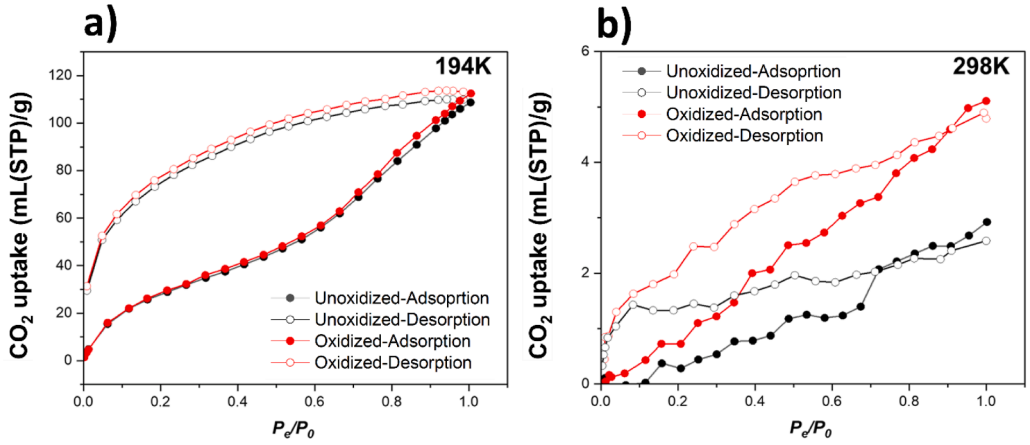

Fig. 8. CO_2 adsorption isotherms of unoxidized and oxidized PLLA microspheres at (a) 194 K and (b) 298 K.

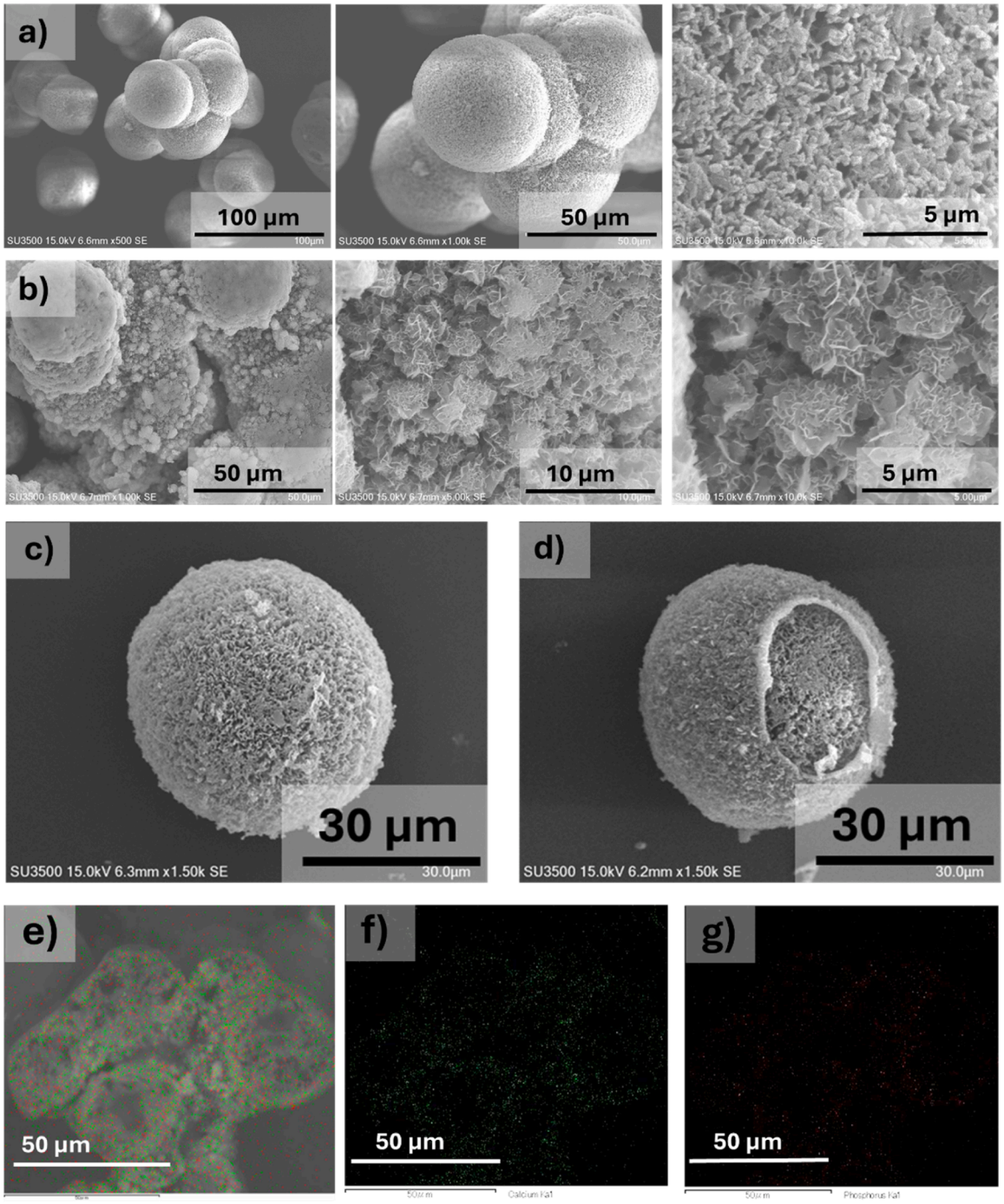

Fig. 8a. SEM images: a,c) unoxidized PLLA microspheres after mineralization and b,d) oxidized PLLA microspheres after mineralization. SEM-EDX images: e) Hydroxyapatite deposition on oxidized PLLA microspheres, f) calcium deposition, and g) phosphorus deposition on the surface of oxidized microspheres.

oxidation time and higher illumination intensity (Table S1). The reduction of molecular weight weakens the interactions between polymer chains [22]. As a result, the oxidized samples exhibited lower thermal stability as seen in TGA measurements. The onset of decomposition temperature for oxidized samples shifted to a lower temperature, from 315 to 285 °C (Fig. 6(a)).

The endothermic behavior of unoxidized and oxidized PLLA microspheres was studied *via* DSC measurements. From the DSC spectra (Fig. 6 (b)), the melting point (T_m) of unoxidized and oxidized microspheres was 149.5 and 149.7 °C, respectively, while crystallinity, X_c, increased from 50.9 to 53.6 %. The enhancement of crystallinity can be attributed to the removal of amorphous molecular chains on PLLA microspheres during crystallization, leaving the more crystalline regions on the microspheres intact. Furthermore, the chain scission that occurred during the oxidation process left behind shorter fragments of polymer chains with higher mobility. As a result, these polymer chains can rearrange and recrystallize into more thermodynamically stable crystalline structures [28].

Furthermore, the degradation behavior of nanoporous PLLA microspheres before and after oxidation was evaluated in PBS buffer solution at 37 °C, and the results are presented in Fig. 7 (a-b) below. The oxidized PLLA microspheres exhibited a higher weight loss of 33 % compared to oxidized PLLA microspheres (13.4 %). In addition, the SEM images revealed considerable structural deterioration of oxidized PLLA

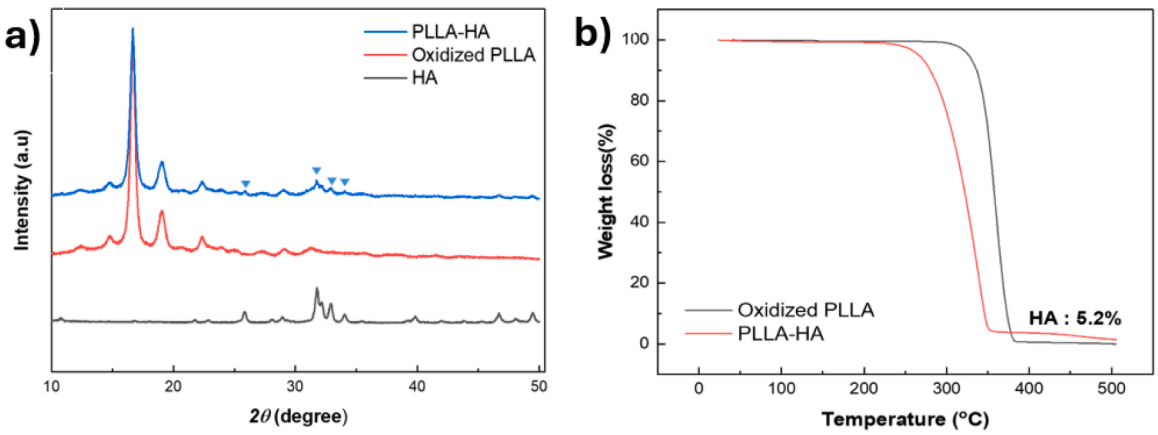

Fig. 9. (a) XRD spectra comparison of hydroxyapatite (HA) and oxidized PLLA before oxidation, and after oxidation (PLLA-HA), and (b) TGA analysis of hydroxyapatite content on PLLA-HA microspheres.

microspheres after 14-day PBS immersion. This accelerated degradation is likely attributed to the improved hydrophilicity of the oxidized PLLA microspheres, arising from the introduction of polar functional groups on the surface, as well as the weakened intermolecular interactions between polymer chains due to the surface oxidation process, as explained earlier.

3.3. CO_2 adsorption properties of nanoporous PLLA microspheres

Fig. 8a-b shows the CO_2 adsorption isotherms of both oxidized and unoxidized nanoporous PLLA microspheres. The CO_2 adsorption capacity of the PLLA microspheres was evaluated at 194 K and 298 K to indirectly assess the success of the surface oxidation process. The oxidized microspheres exhibited a slightly higher CO_2 uptake, adsorbing 113.7 mL/g at 194 K and 5.11 mL/g at 298 K, compared to 110.1 mL/g and 2.8 mL/g, respectively, for the unoxidized microspheres. The slight increase in adsorption capacity observed in the oxidized sample may be attributed to enhanced dipole–quadrupole and electrostatic interactions, facilitated by the presence of polar functional groups on the microsphere surface. These functional groups introduce negatively charged sites that can electrostatically attract the partially positive carbon atom of CO_2 molecules [27]. In short, the presence and reactivity of the polar functional groups on the surface of the PLLA microspheres can be further confirmed due to the enhanced CO_2 adsorption capacity of the PLLA microspheres after oxidation.

3.4. Biomineralization of nanoporous PLLA microspheres

The presence of negatively charged groups such as carboxylic acids and hydroxyls promotes the growth of hydroxyapatite by interacting with calcium cations in SBF solutions [29]. The SEM images in Fig. 9 (a-b) show the surface of oxidized and unoxidized PLLA microspheres after immersion in modified SBF solutions for 7 days. The surface of oxidized PLLA microspheres was covered with spherulitic particles composed of plate-like structures. The hydroxyapatite layer formed a coating on the surface of oxidized PLLA microspheres as shown inFig. 9 (d). In comparison, the surface of unoxidized PLLA microspheres remained bare without the deposition of any obvious spherulitic structures (Fig. c). The diminished porous structure seen in the unoxidized sample might be due to the minimal adsorption of salt on its surface. Such spherulitic crystalline structures are typical of apatite crystals grown from SBF solution, as outlined in many earlier reports [29–31]. As displayed inFig. 9 (e-g), the EDX analysis was performed on the samples to detect the stoichiometric ratio of the hydroxyapatite formed on the surface of PLLA microspheres. The deposition of calcium and phosphorus is evident on the surface of the microsphere. The Ca/P ratio of the mineralized microspheres was 1.58 (Fig. S3), which is comparable to the stoichiometric value of 1.67 for hydroxyapatite crystals [31].

To further analyze the crystal phases of the apatite crystals deposited on the surface of PLLA microspheres, XRD analysis was performed on oxidized PLLA before and after immersion in mSBF solution and compared to commercially obtained hydroxyapatite powder. As shown inFig. 9(a), the mineralized PLLA microspheres clearly showed the presence of hydroxyapatite crystals compared to the bare oxidized PLLA. The peaks arising from hydroxyapatite crystals (located at 26°, 31°, 33°, and 34°) were visible in the spectrum for oxidized PLLA microspheres (PLLA-HA) after immersion in mSBF solution. The presence of similar peaks in both PLLA-HA and hydroxyapatite (HA) spectra confirmed the existence of hydroxyapatite growth on the surface of PLLA microspheres. However, the HA peaks in the FTIR spectra of PLLA-HA were not discernible due to the more robust peaks of PLA (Fig. S2). Additionally, TGA measurements indicated that the hydroxyapatite content on the PLLA microspheres was around 5.2 % (Fig. 9(b)). Overall, these results suggest the feasibility of oxidized nanoporous PLLA microspheres as support for in situ biomineralization of hydroxyapatite using modified simulated body fluid. The oxidized nanoporous PLLA microspheres provided adequate nucleation sites for the successful precipitation of calcium phosphate crystals to form hydroxyapatite on their surface. Hence, the oxidized PLLA microspheres can be a viable candidate to prepare PLLA-hydroxyapatite composite for potential bone engineering scaffolds.

4. Conclusion

In summary, this work outlined a mild and facile method to functionalize the surface of nanoporous PLLA microspheres without significant change to their nanoporous morphology. Polar functional groups were successfully introduced onto the surface of nanoporous microspheres while preserving their nanoporous topology. The effect of oxidation time and illumination intensity on the surface chemical properties of PLLA microspheres was elucidated *via* XPS and dye adsorption measurements. The optimal surface oxidation conditions were determined to be at 60 min oxidation time at 20 mW illumination intensity. The optimization of these oxidation parameters was essential to introduce a sufficient amount of polar functional groups without excessive degradation. Most importantly, the SEM measurements and BET adsorption studies revealed minimal surface degradation of the nanoporous structure after oxidation. Furthermore, the oxidized microspheres showed higher dye and CO_2 adsorption capacity and induced hydroxyapatite growth on their surface through a simple biomineralization process by immersing them in mSBF. All in all, this simple, non-destructive surface oxidation technique provides a new avenue to

functionalize nanoporous polymer scaffolds with significantly enhanced biomineralization ability for potential bone tissue engineering applications.

CRediT authorship contribution statement

Hasinah Rafiq: Writing – original draft, Methodology, Investigation, Formal analysis, Data curation, Conceptualization. **Yu-I Hsu:** Writing – review & editing, Resources, Funding acquisition, Conceptualization. **Hiroshi Uyama:** Supervision, Resources, Project administration, Conceptualization.

Declaration of competing interest

The authors declare that they have no known competing financial interests or personal relationships that could have appeared to influence the work reported in this paper.

Acknowledgments

This work was supported by Japan Science and Technology Agency (JST) PRESTO Grant Number JPMJPR23N4, the Environment Research and Technology Development Fund JPMEERF21S11900 of the Environmental Restoration and Conservation Agency of Japan, and Japan Society for the Promotion of Science (JSPS) KAKENHI Grants (22K21348 and 23K26717). H. R. also would like to thank the Japanese government through the Ministry of Education, Culture, Sports, Science and Technology of Japan (MEXT) for the scholarship. Additionally, we would like to thank Prof. Norimitsu Tohnai and Haojin Li for their help in CO_2 adsorption measurements.

Supplementary materials

Supplementary material associated with this article can be found, in the online version, at doi:10.1016/j.surfin.2025.107514.

Data availability

No data was used for the research described in the article.

References

[1] A.H. Rather, R.S. Khan, T.U. Wani, M.A. Beigh, F.A. Sheikh, Overview on immobilization of enzymes on synthetic polymeric nanofibers fabricated by electrospinning, Biotechnol. Bioeng. 119 (2022) 9–33, https://doi.org/10.1002/bit.27963.

[2] G. Sneddon, A. Greenaway, H.H.P. Yiu, The potential applications of nanoporous materials for the adsorption, separation, and catalytic conversion of carbon dioxide, Adv. Energy Mater. 4 (2014) 1–19, https://doi.org/10.1002/aenm.201301873.

[3] T. Aditya, A. Mesa-Restrepo, A. Civantos, M.K. Cheng, C. Jaramillo-Correa, V. M. Posada, Z. Koyn, J.P. Allain, Ion bombardment-induced nanoarchitectonics on polyetheretherketone surfaces for enhanced nanoporous bioactive implants, ACS Appl. Bio Mater. 6 (2023) 4922–4934, https://doi.org/10.1021/acsabm.3c00642.

[4] D. Ishii, T.H. Ying, A. Mahara, S. Murakami, T. Yamaoka, W.K. Lee, T. Iwata, In vivo tissue response and degradation behavior of PLLA and stereocomplexed PLA nanofibers, Biomacromolecules 10 (2009) 237–242, https://doi.org/10.1021/bm8009363.

[5] Y. Hu, S. Ma, Z. Yang, W. Zhou, Z. Du, J. Huang, H. Yi, C. Wang, Facile fabrication of poly(L-lactic acid) microsphere-incorporated calcium alginate/hydroxyapatite porous scaffolds based on Pickering emulsion templates, Colloids Surfaces B Biointerfaces 140 (2016) 382–391, https://doi.org/10.1016/j.colsurfb.2016.01.005.

[6] T. Watanabe, Y. Kimura, T. Ono, Microfluidic fabrication of monodisperse polylactide microcapsules with tunable structures through rapid precipitation, Langmuir 29 (2013) 14082–14088, https://doi.org/10.1021/la403883a.

[7] S. Mondal, S. Park, J. Choi, T.T.H. Vu, V.H.M. Doan, T.T. Vo, B. Lee, J. Oh, Hydroxyapatite: a journey from biomaterials to advanced functional materials, Adv. Colloid Interface Sci. 321 (2023) 103013, https://doi.org/10.1016/j.cis.2023.103013.

[8] S.S. Manohar, C. Das, V. Kakati, Bone tissue engineering scaffolds: materials and methods, 3D print, Addit. Manuf. 11 (2024) 347–362, https://doi.org/10.1089/3dp.2022.0216.

[9] G. Narayanan, V.N. Vernekar, E.L. Kuyinu, C.T. Laurencin, Poly (lactic acid)-based biomaterials for orthopaedic regenerative engineering, Adv. Drug Deliv. Rev. 107 (2016) 247–276, https://doi.org/10.1016/j.addr.2016.04.015.

[10] K. Szustakiewicz, B. Kryszak, M. Gazińska, J. Chęcmanowski, B. Stępak, M. Grzymajło, A. Antończak, The effect of selective mineralization of PLLA in simulated body fluid induced by ArF excimer laser irradiation: tailored composites with potential in bone tissue engineering, Compos. Sci. Technol. 197 (2020), https://doi.org/10.1016/j.compscitech.2020.108279.

[11] F. Ghorbani, A. Zamanian, A. Behnamghader, M.D. Joupari, Microwave-induced rapid formation of biomimetic hydroxyapatite coating on gelatin-siloxane hybrid microspheres in 10X-SBF solution, E-Polymers 18 (2018) 247–255. https://doi.org/10.1515/epoly-2017-0196.

[12] M. Janmohammadi, M.S. Nourbakhsh, M. Bahraminasab, L. Tayebi, Effect of pore characteristics and alkali treatment on the physicochemical and biological properties of a 3D-printed polycaprolactone bone scaffold, ACS Omega 8 (2023) 7378–7394, https://doi.org/10.1021/acsomega.2c05571.

[13] X. Sun, S. Yang, B. Xue, K. Huo, X. Li, Y. Tian, X. Liao, L. Xie, S. Qin, K. Xu, Q. Zheng, Super-hydrophobic poly (lactic acid) by controlling the hierarchical structure and polymorphic transformation, Chem. Eng. J. 397 (2020) 125297, https://doi.org/10.1016/j.cej.2020.125297.

[14] H. Rafiq, Y.I. Hsu, H. Uyama, Preparation of nanoporous poly (L-lactic acid) microspheres with controllable morphology via thermally-induced phase separation, Polymer 312 (2024) 127622, https://doi.org/10.1016/j.polymer.2024.127622.

[15] P. Chytrosz-Wrobel, M. Golda-Cepa, E. Stodolak-Zych, J. Rysz, A. Kotarba, Effect of oxygen plasma-treatment on surface functional groups, wettability, and nanotopography features of medically relevant polymers with various crystallinities, Appl. Surf. Sci. Adv. 18 (2023) 100497, https://doi.org/10.1016/j.apsadv.2023.100497.

[16] S. Juodkazis, H. Misawa, Controlled through-hole ablation of polymer microspheres, J. Micromechanics Microengineering 14 (2004) 1244–1248, https://doi.org/10.1088/0960-1317/14/8/018.

[17] S. Kim, K.J. Lee, Y. Seo, Surface modification of poly(ether imide) by low-energy ion-beam irradiation and its effect on the polymer blend interface, Langmuir 18 (2002) 6185–6192, https://doi.org/10.1021/la020038k.

[18] M. Tutgun, M.C. Sankir, A. Karatay, E.A. Yildiz, N.A. Karaahmetoglu, A.A. Varsak, C.T. Altaf, Tuning refractive index of PDMS by CO2 laser engraving for polymer optical splitter applications, Mater. Lett. 382 (2025) 137830, https://doi.org/10.1016/j.matlet.2024.137830.

[19] H. Mahjoubi, J.M. Kinsella, M. Murshed, M. Cerruti, Surface modification of poly (d, l -lactic acid) scaffolds for orthopedic applications: a biocompatible, nondestructive route via diazonium chemistry, ACS Appl. Mater. Interfaces 6 (2014) 9975–9987, https://doi.org/10.1021/am502752j.

[20] M.M. El-Baseir, M.A. Phipps, I.W. Kellaway, Preparation and subsequent degradation of poly(L-lactic acid) microspheres suitable for aerosolisation: a physico-chemical study, Int. J. Pharm. 151 (1997) 145–153, https://doi.org/10.1016/S0378-5173(96)04873-9.

[21] J. Ryu, S.H. Ku, H. Lee, C.B. Park, Mussel-inspired polydopamine coating as a universal route to hydroxyapatite crystallization, Adv. Funct. Mater. 20 (2010) 2132–2139, https://doi.org/10.1002/adfm.200902347.

[22] Y. Cao, Y.I. Hsu, H. Uyama, Surface oxidation of poly(ε-caprolactone) using chlorine dioxide radical gas, React. Funct. Polym. 200 (2024), https://doi.org/10.1016/j.reactfunctpolym.2024.105912.

[23] K. Kikkawa, Y.I. Hsu, X. Cui, S. Mizuno, T.A. Asoh, H. Uyama, Surface oxidation of polymer 3D porous structures using chlorine dioxide radical gas, ACS Appl. Polym. Mater 2 (2020) 4964–4972, https://doi.org/10.1021/acsapm.0c00840.

[24] H. Asahara, W. Wu, T.A. Asoh, Y.I. Hsu, T. Inoue, H. Uyama, Surface modification of polylactic acid using a photo-activated chlorine dioxide process: surface properties and dissimilar adhesion, Mater. Adv. 6 (2025), https://doi.org/10.1039/d4ma01275e.

[25] K. Ohkubo, H. Asahara, T. Inoue, Photochemical C-H oxygenation of side-chain methyl groups in polypropylene with chlorine dioxide, Chem. Commun. 55 (2019) 4723–4726, https://doi.org/10.1039/C9CC01037H.

[26] J. Araki, Dye adsorption revisited: application of the cationic dye adsorption method for the quantitative determination of the acidic surface groups of nanocellulose materials, Cellulose 28 (2021) 7707–7715, https://doi.org/10.1007/s10570-021-04035-x.

[27] M. Chen, J. Qiao, X. Sun, W. Chen, H. Uyama, X. Wang, A green and facile strategy for hierarchically porous poly(L-lactic acid)/poly(ε-caprolactone) monolithic composites, J. Mater. Res. 34 (2019) 2990–2999, https://doi.org/10.1557/jmr.2019.214.

[28] S.H. Woo, J.W. Wee, Characterization of accelerated hydrolysis degradation of poly (lactic acid) in phosphate buffered saline solution, Polym. Degrad. Stab. 223 (2024) 110726, https://doi.org/10.1016/j.polymdegradstab.2024.110726.

[29] W.L. Murphy, D.J. Mooney, Bioinspired growth of crystalline carbonate apatite on biodegradable polymer substrata, J. Am. Chem. Soc. 124 (2002) 1910–1917, https://doi.org/10.1021/ja012433n.

[30] F. Ghorbani, A. Zamanian, A. Behnamghader, M. Daliri-Joupari, Bone-like hydroxyapatite mineralization on the bio-inspired PDA nanoparticles using microwave irradiation, Surfaces and Interfaces 15 (2019) 38–42, https://doi.org/10.1016/j.surfin.2019.01.007.

[31] S. Kitahara, Effect of surface hydrolysis of PLA film on apatite formation in vitro, 6 (2008) 77–87.